MOF-directed templating synthesis of a porous multicomponent dodecahedron with hollow interiors for enhanced lithium-ion battery anodes

Sun, Chencheng; Yang, Jun; Rui, Xianhong; Zhang, Weina; Yan, Qingyu; Chen, Peng; Huo, Fengwei; Huang, Wei; Dong, Xiaochen

2015

Sun, C., Yang, J., Rui, X., Zhang, W., Yan, Q., Chen, P., et al. (2015). MOF-directed templating synthesis of a porous multicomponent dodecahedron with hollow interiors for enhanced lithium-ion battery anodes. Journal of Materials Chemistry A, 3(16), 8483-8488.

https://hdl.handle.net/10356/82055

https://doi.org/10.1039/C5TA00455A

Journal Name

RSCPublishing

ARTICLE

MOF-directed templating synthesis of porous multicomponent dodecahedron with hollow interiors for enhanced lithium-ion battery anodes

Cite this: *DOI: J . Mater. Chem. A,2015,3,8483*

Received 20th January 2015
Accepted 9th March 2015

DOI: 10.1039/c5ta00455a

www.rsc.org/MaterialsA

Chencheng Sun,[a] Jun Yang,[a] Xianhong Rui,[b] Weina Zhang,[b] Qingyu Yan,[b] Peng Chen,[c] Fengwei Huo,[a] Wei Huang*[a] and Xiaochen Dong*[a]*

The high performance of Lithium-ion battery (LIB) electrode relies largely on meticulous design of hierarchical nanostructures with optimal balance between superior electrochemical properties and conductivity. Herein, we present a facile and cost-effective solvothermal method to fabricate porous $NiCo_2O_4$/NiO hollow dodecahedron using zeolitic imidazolate framework-67 (ZIF-67) as both precursor and self-sacrificing template. Accurate control between the template etching and the precipitation of the shells is crucial to the preparation of the perfect nanocages. Serving as LIB anode materials, such metal-organic frameworks derived multiple transition metal oxides demonstrate a high revisable capacity of 1535 mAh g^{-1} at 0.2 A g^{-1} and a good cycling stability (97.2% retention after 100 cycles). The presented strategy represents a general route to synthesize various hierarchically interconnected and porous nanostructures of mixed transition metal oxides which are promising for a range of applications.

1. Introduction

Hollow nanostructures with large surface-to-volume ratio and interconnected pathways for both electrons and ions are of great significance to a wide range of applications, such as energy storage and conversion, catalysis, sensing, and biomedicine.[1-7] Recently, several novel strategies have been developed to fabricate anisotropic hollow structures based on different principles, including Kirkendall effect,[8, 9] galvanic replacement,[10] chemical etching,[11] ionic exchange[12] and self-assembly[13, 14]. For example, templating-engaged methods based on galvanic replacement or chemical etching have been considered as the most representative and facile approach toward hollow structures, which involve the controlled assembling of the desired shells on the basis of hard-/soft-template.[15, 16] Such approaches are very effective to form hollow particles with various shapes, yet their versatility still suffer from many difficulties, ranging from the formation of uniform coatings around high-curvature surfaces to completely removal of the template after reaction. [17, 18]

Metal-organic frameworks (MOFs) synthesized by assembling metal-ions with organic ligands into an infinite array, are a new class of porous materials that have shown promising applications in gas storage, catalysis, sensing and separation.[19-23] Motivated by their ultrahigh surface area, tunable pores and chemical tunability, MOFs have recently attracted immense interests for serving as self-sacrificial templates to synthesize porous binary transition metal oxides, such as ZnO,[24, 25] Fe_2O_3,[26, 27] Co_3O_4,[28] and Cu_xO[29]. As compared to other templated-strategies, the MOFs-derived metal oxides often demonstrate special structural features, such as large surface area, hierarchical pore sizes and a hydrophobic surface.[30, 31] In spite of many reports on MOFs-derived metal oxide composites and their applications,[32, 33] this emerging area is characterized by significant challenges, several of which we address here. First, the rational design and fabrication of multiple transition metal oxide with nonspherical hollow interiors is still in its infancy, likely due to high residual stress induced by combining materials with distinct physicochemical properties.[34] To date, only a few illustrations, including $Zn_xCo_{3-x}O_4$,[35] $NiFe_2O_4/Fe_2O_3$[36] and $ZnO/ZnFe_2O_4/C$[37] have been reported, all focusing on mixed transition metal oxides with spinel-like structures due to their several orders higher electrical conductivity and more electrochemical activity sites than simple transition metal oxides.[38, 39] Second, the ability to accurate control the shape of such nonspherical hollow structure is highly desirable. Reaction conditions such as solvent composition and temperature are crucial for the fabrication of perfect hollow structure, as both of them have great influence on the balance between the dissolution rate of template and the precipitation of shell.[40, 41] For example, by controlling the diffusion rate of the titanium coordination ion as well as the calcination process, Wang et al.[42] synthesized the

uniform multishelled TiO_2 hollow spheres with different shell number and interior structures. Third, traditional mixing technologies such as mechanical agitation, supercritical fluid are difficult to uniformly mixed multicomponent.[43] Therefore, it is necessary to seek a new way to improve the uniformity degree. Homogeneous mixing the multicomponent within the shell even in atomic scale can help a battery hold its charge longer and re-charge at a faster rate.[44]

Here, in order to address the above difficulties, we demonstrate a facile and cost-effective synthesis of porous multicomponent *via* MOF-templated reactions. By deliberately controlling the balance between the dissolution rate of MOF and the precipitation rate of shell, porous $NiCo_2O_4$/NiO hollow dodecahedron ($NiCo_2O_4$/NiO-HD) can be obtained. LIB anode made from this novel material exhibits high capacity and cycling stability. It outperforms other cobalt-based metal oxide LIBs anodes.

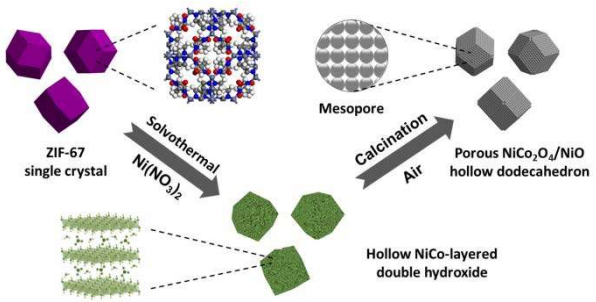

Fig. 1 Schematic illustration for the preparation process of porous $NiCo_2O_4$/NiO hollow dodecahedron (HD).

2. Experimental section

Materials and reagents

Cobalt nitrate hexahydrate (> 98%), 2-methylimidazole (99%) and nickel nitrate (> 98.5%) were obtained from Sigma-Aldrich. Methanol (99.99%) and absolute ethanol (99.99%) were obtained from Fisher Scientific. All chemical were used as obtained without further purification.

Synthesis of Zeolitic Imidazolate Framework 67 (ZIF-67) single nanocrystals

ZIF-67 was prepared according to the reported method.[1] Specifically, 249.0 mg (1.0 mmol) cobalt nitrate hexahydrate or 328.0 mg (4.0 mmol) 2-methylimidazole was dissolved in 25.0 mL methanol. These two solutions were then mixed followed by 24h incubation at room temperature. The resulting ZIF-67 single nanocrystals were collected by several rinse-centrifugation cycles and vacuum-dried overnight.

Synthesis of porous $NiCo_2O_4$/NiO hollow dodecahedra ($NiCo_2O_4$/NiO-HD) and Co_3O_4-HD

The as-prepared ZIF-67 powder was transferred into a 40 mL glass bottle containing 150 mg nickel nitrate and 25.0 mL absolute ethanol (32.8 mM). The sample was then heated in an oven at 90 °C for 1 h. The greenish product was harvested by centrifugation, following by washing with anhydrous methanol and vacuum-drying overnight. The obtained product was subsequently calcinated at 400 °C in air for 1 h with a heating rate of 2 °C min^{-1} to finally generate $NiCo_2O_4$/NiO-HD. For comparison, Co_3O_4-HD was also prepared according to the reported method.[2] Briefly, the powder of ZIF-67 was placed in a tube furnace and heated to 500 °C with a ramping rate of 2 °C min^{-1}. The sample was calcinated at 350 °C in flowing air for 1 h.

Characterization

X-ray diffraction (XRD) patterns were collected on a Bruker D8 Advanced X-ray diffractometer with Ni filtered Cu Kα radiation (λ= 1.5406 Å) at a voltage of 40 kV and a current of 40 mA. The morphology of the products were acquired from field-emission scanning electron microscope (FESEM, JEOL JSM-7600F) and transmission electron microscopy (TEM JEOL JSM-2100F). Energy-dispersive X-ray (EDX) analysis and elemental mapping were performed using the EDX spectroscopy attached to the JEM-2100F. X-ray photoelectron spectra (XPS) were obtained using an Axis Ultra (Kratos Analytical, UK) XPS spectrometer equipped with an Al Kαsource (1486.6 eV). Thermogravimetric analysis (TGA) was measured using a Shimadzu-60 Thermogravimetric Analyzer in Air, over a range from room temperature to 600 °C with a ramp of 2 °C min^{-1}. The nitrogen adsorption-desorption isotherms of the samples were measured at 77K using a Tri-star 3020 accelerated surface area and porosimetry system. The specific surface areas were determined based on Brunauer-Emmett-Teller (BET) method from nitrogen adsorption data in the relative pressure range from 0.05 to 0.20. The regression coefficients (R^2) of the linear part is above 0.99. Total pore volume was calculated from the amount of gas adsorbed at the relative pressure of 0.99. Pore size distribution was derived from adsorption branches by the Barrett-Joyner-Halenda (BJH) method.

Electrochemical Measurements

Electrochemical measurements were carried out at room temperature based on a coin-type half-cell configuration. The working electrode was fabricated by mixing active materials, super-P carbon black and polyvinylidene fluoride (PVDF) in a weight ratio of 80:10:10 in N-methyl-2 pyrrolidinone (NMP) solvent. The resulting slurry was coated onto Cu foil and dried at 60 °C for 12 h. The coin cells were assembled in argon-filled glove box with moisture and oxygen concentrations less than 1ppm by using lithium metal as counter electrode, Celgard 2400 membrane as the separator, and 1 M $LiPF_6$ in a mixture of ethylene carbonate and dimethyl carbonate (1:1 in volume) as the electrolyte. The cell were tested on a NEWARE multichannel battery test system with galvanostatic charge and discharge (voltage window of 0.01-3.0 V). Cyclic voltammetry was carried out on a Solartron Analytical instrument (AMETEK model 1470E) at a scan rate of 0.2 mV s^{-1} between 0.01 and 3.0 V. The electrode loading for each battery is about 0.5mg±0.1mg.

3. Results and Discussion

As illustrated in **Fig. 1**, ZIF-67 single crystals with a hollow dodecahedron shape were employed as both precursor and self-sacrificing template to obtain hollow dodecahedron of NiCo layered double hydroxide (NiCo-LDH-HD). After calcination in air for 1h, porous $NiCo_2O_4$/NiO-HD was obtained.

ZIF-67 purple solution can be obtained by mixing coalt nitrate and 2-methylimidazole in methanol with the mixture being aged under ambient conditions for 24 h.[30] (Fig. 2a). The measured X-ray diffraction (XRD) pattern of as-synthesized ZIF-67 agrees well with the simulated pattern (Figure S1a) based on the well-accepted crystalline model of ZIF-67[45] (Fig. 2b). As revealed by field-emission scanning electron microscopy (FESEM), ZIF-67 crystals have a uniform size ~500 nm with smooth surface and defined dodecahedral structure (Fig. 2c). Transmission electron microscopy (TEM) suggests that ZIF-67 particles are solid (Fig. 2d).

Under solvothermal (ST) condition in absolute ethanol as well as the presence of $Ni(NO_3)_2$, NiCo-LDH-HD particles were produced as evidenced by fading of original purple color and appearance of greenish precipitation (Fig. 2e). SEM shows that the obtained products inherit the morphology of ZIF-67 with high fidelity (Fig. 2f). As Characterized by TEM, NiCo-LDH particles are hollow (Fig. 2g) and assembled by ultrathin sheets (Fig. 2h). The selected area electron diffraction (SAED) pattern indicates the polycrystalline nature of NiCo-LDH-HD. The XRD pattern matches well with that of NiCo-LDH (Figure S1b).[46]

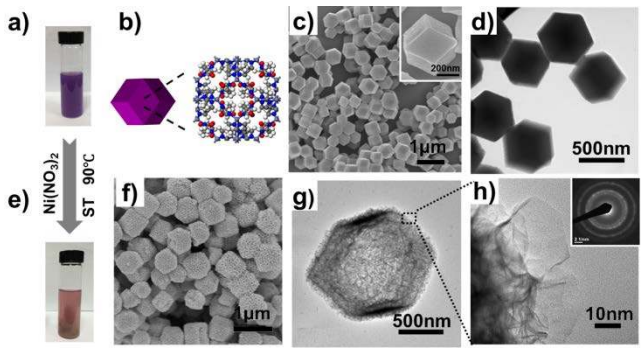

Fig. 2 (a) Digital photo of ZIF-67 solution. (b) Geometrical and crystal structural models of ZIF-67. (c) Low- and high-magnified (inset) FESEM images and (d) TEM image of ZIF-67. (e) Digital photo of NiCo-LDH-HD particles. (f) FESEM images of NiCo-LDH-HD particles. (g) TEM images of NiCo-LDH-HD after solvothermal treatment with $Ni(NO_3)_2$. (h) High magnified TEM image and corresponding SAED pattern of NiCo-LDH-HD nanoparticles.

The reaction system is relatively simple, driven hydrolysis of $Ni(NO_3)_2$ in absolute ethanol, ZIF-67 slowly dissolves and the released Co^{3+} ions co-precipitate with Ni^{2+} ions to form NiCo-LDH nanosheets on the template. Therefore, an accurate control of the balance between the rates of ZIF-67 template etching and NiCo-LDH formation is critical to attain perfect hollow dodecahedral structure. To illustrate this, we show that a small amount of $Ni(NO_3)_2$ (less than 100 mg, 22 mM) leads to the formation of solid particles due to insufficient template dissolution, whereas 500 mg (110 mM) $Ni(NO_3)_2$ leads to the formation of flower-like structure due to rapid collapse of the template (Figure S2). Only appropriate concentration of $Ni(NO_3)_2$ (100-125 mg, 22 mM~33 mM) leads to a shrinked ZIF-67 core, charactered by TEM, whose identity is verified by XRD (Figure S3). To insure a mild rate of $Ni(NO_3)_2$ hydrolysis, abolute ethanol is used as solvent in this reaction. The hollow dodecahedral structure of NiCo-LDH collapses from nanoflowers to nanosheets with the increseasment of DI water because ZIF-67 dissovles rapidy by the drastic hydrolysis (Figure S4). Using ethnol as solvent and appropriate amount of $Ni(NO_3)_2$, better crytallinity and larger grain size can be obtained as evidenced by more prominent and sharp XRD peaks (Figure S5).

The as-prepared NiCo-LDH-HD was further transformed into the porous hybrid $NiCo_2O_4$/NiO-HD at 400 °C in air atmosphere at a heating rate of 2 °C min^{-1}. As confirmed by the thermogravimetric (TG) analysis (Figure S6), after the initial loss (~4 wt.%) of adsorbed and coordinated water molecules,[47] a steep weight loss (~34.7 wt%) starts beyond ~200 °C due to decomposition of NiCo-LDH-HD. Hence, annealing the as-prepared LDH-HD at 400 °C in air flow for 1 h is sufficient to ensure complete conversion from NiCo-LDH-HD to $NiCo_2O_4$/NiO-HD. FESEM (Fig. 3a) and TEM (Fig. 3b and c) reveal that the obtained $NiCo_2O_4$/NiO-HD structures are porous and hollow dodecahedron consitituted by individual nanoparticles (NPs) of ~10 nm in diameter. The formation of NPs and porous surface is resulted from recrystallization process and the release of gas molecules.[18] Furthermore, the lattice fringes can be clearly seen in the high-resolution TEM (HRTEM) image (Fig. 3d), in which 2.45 Å can be assigned to the (311) interplane spacing of $NiCo_2O_4$ while 1.48 Å matches well with the spacing of the (110) planes of NiO. The well-defined rings of electron diffraction pattern can be indexed to various crystalline planes, confirming the polycrystallinity of $NiCo_2O_4$/NiO (Fig. 3e). Moverover, the elemental mapping results (Fig. 3f) demonstrate the uniform distribution of Ni and Co within the HD structure. The above observations indicate that the two types of metal oxides ($NiCo_2O_4$ and NiO) are seamlessly integrated at atomic scale.

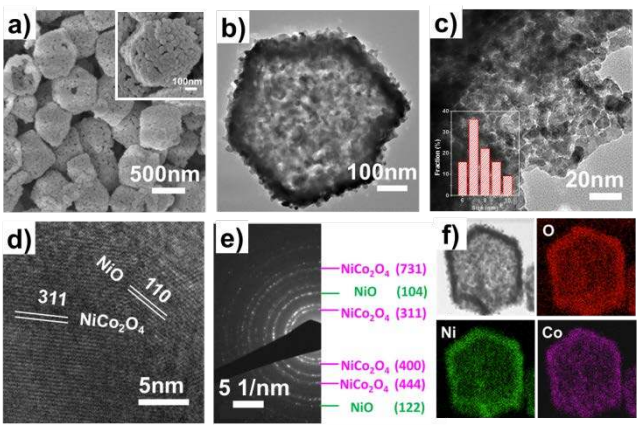

Fig. 3 Structure characterization of $NiCo_2O_4$/NiO HD particles. (a) low- and high-magnified (insert) FESEM images. (b) Low-magnified TEM image. and (c) High-magnified TEM images and corresponding particle size distribution (inset). (d) HRTEM image. (e) SAED pattern. (f) EDX-elemental mapping of O, Ni, Co.

The crystallinity and co-existence of two kinds of metal oxides are further confirmed by XRD as the results shown in Fig. 4a. The diffraction peaks can be indexed to cubic $NiCo_2O_4$ (Fd-3m, a=b=c=0.811 nm) and hexagonal NiO (R-3m, a=b=0.296 nm, c=0.723 nm). Energy-dispersive X-ray spectroscopy (EDX) analysis indicates the atomic ratio (Ni/Co) of ~1.16 (Fig. 4b), corresponding to 43 at.% $NiCo_2O_4$ and 57 at.% NiO. Brunauer-Emmett-Teller (BET) surface area of the porous $NiCo_2O_4$/NiO-HD is measured to be 126.3 $m^2 g^{-1}$ (Fig. 4c), and both meso- and micro- pore existed in the HD (Fig. 4c inset). It is expected that this porous 3D hollow architecture can not only offer abundant active sites and fast charge transport, but also help buffer the volume expansion/contraction upon cycling.[48]

The carbon peak in the X-ray photoelectron (XPS) spectrum of $NiCo_2O_4$/NiO-HD is absent, indicating the full oxidation from NiCo-LDH to $NiCo_2O_4$/NiO-HD (Figure S7). In the high-resolution XPS spectrum, the Ni 2p spectrum can be fitted with two spin-orbit doublets (characteristic of Ni^{2+} and Ni^{3+}) and two shakeup satellites (Fig. 4d). The Co 2p spectrum is fitted with two spin-orbit doublets (characteristic of Co^{2+} and Co^{3+}) and two shakeup satellites (Fig. 4e). The atomic ratio of Ni to Co is ~1.16, identical to the EDX results. The O 1s spectrum exhibits four oxygen bonding features (Fig. 4f). The O1 and O2 peaks at ~529.5 eV are typical of the metal-oxygen bond.[49] The O3 peak at ~531.2 eV is commonly associated with defects, chemisorbed oxygen or under-coordinated lattice oxygen.[50] The O4 peak is weak, suggesting the negligible amount of physisorbed or chemisorbed waters on the surface.[51] Taken together, these results show that $NiCo_2O_4$/NiO-HD contains Ni^{2+}, Ni^{3+}, Co^{2+}, Co^{3+} and O^{2-}, consistent with the previously reported observations.[52, 53]

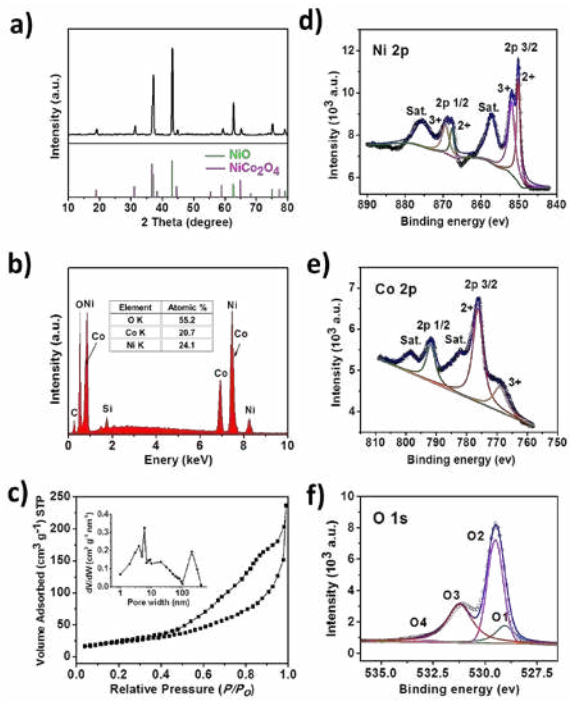

Fig. 4 Characteristics of the as-prepared porous $NiCo_2O_4$/NiO HD. (a) XRD pattern. (b) EDX spectrum. (c) N_2-sorption isotherms and corresponding pore-size distribution (inset). (d-f) High-resolution XPS spectra of Ni 2p, Co 2p, and O 1s, respectively.

As a case study, the potential of $NiCo_2O_4$/NiO-HD as the anode material of LIB was explored. Fig. 5a shows the cyclic votammograms (CVs) of the porous $NiCo_2O_4$/NiO-HD electrode for the 1st, 2nd and 5th cycles. A pronounced peak at 0.38 V during the first cathodic scan, which can be attributed to the decomposition of $NiCo_2O_4$/NiO and the alloying reaction between Li and Ni, respectively.[54] On the first anodic sweep, one broad peak at around 1.5 V and a shoulder at higher potentials can be observed, indicating the re-oxidation of Ni and Co. From the second cycle onwards, the cathodic peak is shifted to 0.89 V due to the partial reduction of Co^{3+} to Co^{2+}. Evidently, the CV profiles overlap very well from the second cycle onwards as they do not change significantly upon further sweeps, suggesting highly reversible electrochemical reactions.[55] Compared with $NiCo_2O_4$/NiO, the CV curves of ZIF-67 derived Co_3O_4 show only one pair of redox peak and the gradually decline of the current intensity indicate the poor cycle performance of Co_3O_4. Fig. 5b shows the galvanostatic charge/discharge curves of the $NiCo_2O_4$/NiO-HD electrode at the 1st, 3rd, 50th or 100th cycle at a current density of 0.2 A g^{-1} over a potential range between 0.01 and 3.0 V (*vs.* Li^+/Li). The obvious plateau at ~0.75 V in the initial discharge curve corresponds to the decomposition of $NiCo_2O_4$ and NiO into Ni^0, Co^0, and Li_2O.[56] The initial discharge/charge capacities are ~1622 and ~1030 mAh g^{-1} respectively, indicating a low irreversible capacity loss of ~36.5%. This capacity loss may result from the incomplete conversion reaction and irreversible lithium loss due to the formation of a solid-electrolyte-interface (SEI) layer.[57] From the second cycle onwards, the Coulombic efficiency of the $NiCo_2O_4$/NiO electrode remains nearly 100%, and its capacity reaches 1497 mAh g^{-1} over 100 cycles at a current density of 0.2 A g^{-1}. The gradually increasing reversible capacity during cycling is a common phenomenon for metal-oxide electrode materials, attributable to a gradual activation process of the metal-oxide electrodes as well as reversible reactions between metal particles and electrolytes.[58, 59] Fig. 5c depicts the discharge capacity as a function of cycle number at a constant current density of 0.2 A g^{-1}. The capacity of $NiCo_2O_4$/NiO-HD increases with cycling with ~100% Coulombic efficiency. Remarkably, the commonly observed capacity degradation due to structrual damage caused by Li ion insertion/desertion is absent. For comparison, ZIF-67 derived Co_3O_4-HD is also synthesized. Although Co_3O_4-HD is also hollow dodecahedron (Figure S9), its capacity is much smaller and decays quickly with cycling as compared with $NiCo_2O_4$/NiO-HD (Fig. 5c). It is, at least in part, due to the poor conductivity of the former. This is supported by the the electrochemical impedance spectroscopy (EIS) measurements which show that the $NiCo_2O_4$/NiO-HD electrode exhibits a much smaller charge transfer resistance (a negligible radius of the preceding semicircle of the Nyquist plot) than Co_3O_4-HD electrode (Figure S10). Furthermore, our hierarchical $NiCo_2O_4$/NiO-HD offers higher capacity and enhanced cycling stability than the previously reported cobalt-based metal oxides derived by MOF or other methods (Table S1). The practical use of LIBs requires fast discharge and/or charge rates.[17] As shown

in Fig. 5d, even at a high current density of 10 A g^{-1}, the specific capacity retains at 689 mAh g^{-1}, which is still far better than the theoretical capacity of graphite (372 mAh g^{-1}). Moreover, when the current density is reduced back to 0.5 A g^{-1}, a capacity of ~1223 mAh g^{-1} is attained (larger than the initial value at the same current level). The rate performance of $NiCo_2O_4$/NiO-HD is superior to the previously reported MOF-derive metal oxides, such as, Fe_2O_3, [60] Co_3O_4[34], and $ZnMn_2O_4$.[61]

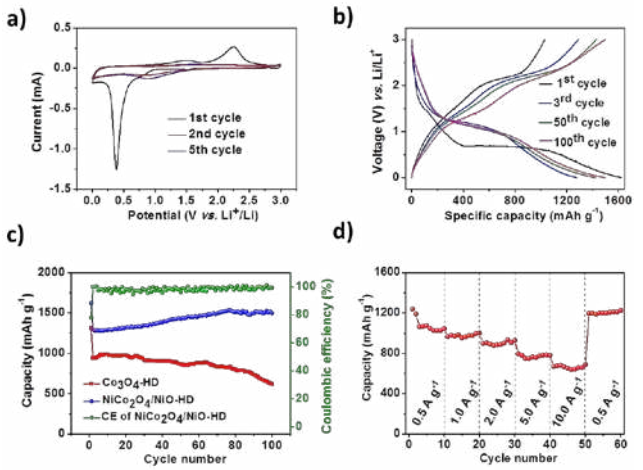

Fig. 5 Electrochemical performance of the electrode made of the porous $NiCo_2O_4$/NiO-HD. (a) Representative cyclic voltammograms of $NiCo_2O_4$/NiO-HD at a scan rate of 0.1 mV s^{-1} between 0.01 and 3 V *vs.* Li/Li^+. (b) Charge-discharge profiles at a current density of 0.2 A g^{-1} for the 1st, 3rd, 50th and 100th cycles. (c) Cycling performance of $NiCo_2O_4$/NiO-HD and Co_3O_4-HD at a current density of 0.2 A g^{-1}. (d) Rate capabilities and Coulombic efficiency at various current densities of 0.5, 1, 2, 5, 10 A g^{-1}, respectively.

4. Conclusions

In summary, by using MOF as both precursor and sacrificial template, we have demonstrated a facile and controllable synthesis of a porous $NiCo_2O_4$/NiO-HD with an exquisite nanostructure, which is a hollow dodecahedron hierarchically assembled by numerous nanoparticles (~10 nm in size). It was found that the dissolution rate of MOF and the precipitation rate of shell adjusted *via* the amount of metal salts and solvent composition determine the finally morphology of the products. This novel multiple nanomaterial shall promise a range of novel applications. As a case study, we present its use as LIB anode. Its exceptional performance (capacity, cycling stability, rating property) could be ascribed to the following reasons. Firstly, its unique hierarchical nanoarchitecture provides large surface area, high mechanical tolerance to volume expansion caused by Li ion insertion, and easy pathways for electron transport and ion diffusion. Secondly, as compared with other metal oxide compounds, $NiCo_2O_4$/NiO-HD offers both high electrochemical activities and good conductivity. The present route is not only facile but also cost-effective, and therefore it is highly promising for scaled-up production. As the metal ions and hydrolysis rate of MOFs are easily tunable, we do believe that this facile MOF-directed templating strategy can be extended to prepare other hollow multicomponent electrode materials with outstanding performance for next-generation energy-storage devices.

Acknowledgements

The project was supported by Jiangsu Provincial Founds for Distinguished Young Scholars (BK20130046, BK20140044), the NNSF of China (21275076, 61328401), Program for New Century Excellent Talents in University (NCET-13-0853), Qing Lan Project, National Synergistic Innovation Center for Advanced Materials (SICAM), Synergetic Innovation Center for Organic Electronics and Information Displays, the Priority Academic Program Development of Jiangsu Higher Education Institutions (PAPD), SERC Grant (#102170 0142) from the Agency for Science, Technology and Research (A*STAR, Singapore).

Notes and references

[a] Key Laboratory of Flexible Electronics (KLOFE) & Institute of Advanced Materials (IAM), Jiangsu National Synergistic Innovation Center for Advanced Materials (SICAM), Nanjing Tech University (Nanjing Tech), 30 South Puzhu Road, Nanjing, 211816, China

[b] School of Materials Science and Engineering, Nanyang Technological University, 50 Nanyang Avenue, 639798, Singapore

[c] School of Chemical and Biomedical Engineering, Nanyang Technological University, 62 Nanyang Drive, 637459, Singapore

† Electronic Supplementary Information (ESI) available: [details of any supplementary information available should be included here]. See DOI: 10.1039/b000000x/

1. X. Lai, J. E. Halpert and D. Wang, *Energy Environ. Sci.*, 2012, 5, 5604-5618.
2. L. Pan, A. Chortos, G. Yu, Y. Wang, S. Isaacson, R. Allen, Y. Shi, R. Dauskardt and Z. Bao, *Nat. commun.*, 2014, 5.
3. E. González, J. Arbiol and V. F. Puntes, *Science*, 2011, 334, 1377-1380.
4. J. Nai, Y. Tian, X. Guan and L. Guo, *J. Am. Chem. Soc.*, 2013, 135, 16082-16091.
5. X. W. D. Lou, L. A. Archer and Z. Yang, *Adv. Mater.*, 2008, 20, 3987-4019.
6. X. Lai, J. Li, B. A. Korgel, Z. Dong, Z. Li, F. Su, J. Du and D. Wang, *Angew. Chem.*, 2011, 123, 2790-2793.
7. D. Yang, X. Kang, P. a. Ma, Y. Dai, Z. Hou, Z. Cheng, C. Li and J. Lin, *Biomaterials*, 2013, 34, 1601-1612.
8. Y. Yin, R. M. Rioux, C. K. Erdonmez, S. Hughes, G. A. Somorjai and A. P. Alivisatos, *Science*, 2004, 304, 711-714.
9. Y. Yu, X. Yin, A. Kvit and X. Wang, *Nano Lett.*, 2014, 14, 2528-2535.
10. X. Xia, Y. Wang, A. Ruditskiy and Y. Xia, *Adv. Mater.*, 2013, 25, 6313-6333.
11. M. Hu, S. Furukawa, R. Ohtani, H. Sukegawa, Y. Nemoto, J. Reboul, S. Kitagawa and Y. Yamauchi, *Angew. Chem.*, 2012, 124, 1008-1012.
12. S. Xiong and H. C. Zeng, *Angew. Chem. Int. Ed.*, 2012, 51, 949-952.

13. R. Rakhi, W. Chen, D. Cha and H. Alshareef, *Nano Lett.*, 2012, 12, 2559-2567.
14. X. Rui, H. Tan, D. Sim, W. Liu, C. Xu, H. H. Hng, R. Yazami, T. M. Lim and Q. Yan, *J. Power Sources*, 2013, 222, 97-102.
15. S. Xu, C. M. Hessel, H. Ren, R. Yu, Q. Jin, M. Yang, H. Zhao and D. Wang, *Energy Environ. Sci.*, 2014, 7, 632-637.
16. F. Caruso, R. A. Caruso and H. Möhwald, *Science*, 1998, 282, 1111-1114.
17. M. Hu, J. Chen, Z.-Y. Li, L. Au, G. V. Hartland, X. Li, M. Marquez and Y. Xia, *Chem. Soc. Rev.*, 2006, 35, 1084-1094.
18. L. Hu and Q. Chen, *Nanoscale*, 2014, 6, 1236-1257.
19. S. Kitagawa, *Chem. Soc. Rev.*, 2014, 43, 5415-5418.
20. H. Li, M. Eddaoudi, M. O'Keeffe and O. M. Yaghi, *Nature*, 1999, 402, 276-279.
21. Y. Cui, Y. Yue, G. Qian and B. Chen, *Chem. Rev.*, 2011, 112, 1126-1162.
22. G. Lu, S. Li, Z. Guo, O. K. Farha, B. G. Hauser, X. Qi, Y. Wang, X. Wang, S. Han, X. Liu, J. S. DuChene, H. Zhang, Q. Zhang, X. Chen, J. Ma, S. C. Loo, W. D. Wei, Y. Yang, J. T. Hupp and F. Huo, *Nat. chem.*, 2012, 4, 310-316.
23. W. Zhang, G. Lu, C. Cui, Y. Liu, S. Li, W. Yan, C. Xing, Y. R. Chi, Y. Yang and F. Huo, *Adv. Mater.*, 2014, DOI: 10.1002/adma.201400620.
24. S. J. Yang, S. Nam, T. Kim, J. H. Im, H. Jung, J. H. Kang, S. Wi, B. Park and C. R. Park, *J. Am. Chem. Soc.*, 2013, 135, 7394-7397.
25. R. Li, X. Ren, X. Feng, X. Li, C. Hu and B. Wang, *Chem. Commun.*, 2014, 50, 6894-6897.
26. S. Qiu, M. Xue and G. Zhu, *Chem. Soc. Rev.*, 2014, 43, 6116-6140.
27. B. Kong, J. Tang, Z. Wu, J. Wei, H. Wu, Y. Wang, G. Zheng and D. Zhao, *Angew. Chem. Int. Ed.*, 2014, 53, 2888-2892.
28. T. Y. Ma, S. Dai, M. Jaroniec and S. Z. Qiao, *J. Am. Chem. Soc.*, 2014, 136, 13925-13931.
29. A. Banerjee, U. Singh, V. Aravindan, M. Srinivasan and S. Ogale, *Nano Energy*, 2013, 2, 1158-1163.
30. F. Zheng, Y. Yang and Q. Chen, *Nature communications*, 2014, 5, 5261.
31. Y. Han, P. Qi, S. Li, X. Feng, J. Zhou, H. Li, S. Su, X. Li and B. Wang, *Chem. Commun.*, 2014, 50, 8057-8060.
32. S.-L. Li and Q. Xu, *Energy Environ. Sci.*, 2013, 6, 1656-1683.
33. J.-K. Sun and Q. Xu, *Energy Environ. Sci.*, 2014, DOI: 10.1039/c4ee00517a.
34. R. Wu, X. Qian, X. Rui, H. Liu, B. Yadian, K. Zhou, J. Wei, Q. Yan, X. Q. Feng and Y. Long, *Small*, 2014, 10, 1932-1938.
35. R. Wu, X. Qian, K. Zhou, J. Wei, J. Lou and P. M. Ajayan, *ACS nano*, 2014.
36. G. Huang, F. Zhang, L. Zhang, X. Du, J. Wang and L. Wang, *J. Mater. Chem. A*, 2014, 2, 8048-8053.
37. F. Zou, X. Hu, Z. Li, L. Qie, C. Hu, R. Zeng, Y. Jiang and Y. Huang, *Adv. Mater.*, 2014, 26, 6622-6628.
38. C. Yuan, H. B. Wu, Y. Xie and X. W. D. Lou, *Angew. Chem. Int. Ed.*, 2014, 53, 1488-1504.
39. X.-C. Dong, Z. Yufei, L. Li, S. Haiquan and H. Wei, *J. Mater. Chem. A*, 2014, DOI: 10.1039/c4ta04996a.
40. W.-w. Zhan, Q. Kuang, J.-z. Zhou, X.-j. Kong, Z.-x. Xie and L.-s. Zheng, *J. Am. Chem. Soc.*, 2013, 135, 1926-1933.
41. Z. Jiang, Z. Li, Z. Qin, H. Sun, X. Jiao and D. Chen, *Nanoscale*, 2013, 5, 11770-11775.
42. H. Ren, R. Yu, J. Wang, Q. Jin, M. Yang, D. Mao, D. Kisailus, H. Zhao and D. Wang, *Nano Lett.*, 2014, 14, 6679-6684.
43. N. Fan, X. Li, H. Li, C. Sun, D. Kong and Y. Qian, *J. Power Sources*, 2013, 223, 114-118.
44. M.-K. Song, S. Park, F. M. Alamgir, J. Cho and M. Liu, *Materials Science and Engineering: R: Reports*, 2011, 72, 203-252.
45. N. Yanai, M. Sindoro, J. Yan and S. Granick, *J. Am. Chem. Soc.*, 2012, 135, 34-37.
46. F. Song and X. Hu, *Nat. commun.*, 2014, 5.
47. M. E. Kosal, J.-H. Chou, S. R. Wilson and K. S. Suslick, *Nature materials*, 2002, 1, 118-121.
48. D. Yang, Z. Lu, X. Rui, X. Huang, H. Li, J. Zhu, W. Zhang, Y. M. Lam, H. H. Hng and H. Zhang, *Angew. Chem.*, 2014, 126, 9506-9509.
49. J. Marco, J. Gancedo, M. Gracia, J. Gautier, E. Rıos and F. Berry, *J. Solid State Chem.*, 2000, 153, 74-81.
50. Y. E. Roginskaya, O. Morozova, E. Lubnin, Y. E. Ulitina, G. Lopukhova and S. Trasatti, *Langmuir*, 1997, 13, 4621-4627.
51. T. Choudhury, S. Saied, J. Sullivan and A. Abbot, *J. Phys. D: Appl. Phys.*, 1989, 22, 1185.
52. H. S. Jadhav, R. S. Kalubarme, C.-N. Park, J. Kim and C.-J. Park, *Nanoscale*, 2014, 6, 10071-10076.
53. L. Huang, D. Chen, Y. Ding, S. Feng, Z. L. Wang and M. Liu, *Nano Lett.*, 2013, 13, 3135-3139.
54. G. Gao, H. B. Wu and X. W. D. Lou, *Adv. Energy Mater.*, 2014.
55. S. Yuan, X.-l. Huang, D.-l. Ma, H.-g. Wang, F.-z. Meng and X.-b. Zhang, *Adv. Mater.*, 2014, 26, 2273-2279.
56. L. Wang, L. Zhuo, C. Zhang and F. Zhao, *ACS appl. mater. interfaces*, 2014, 6, 10813-10820.
57. H. Wu, G. Chan, J. W. Choi, Y. Yao, M. T. McDowell, S. W. Lee, A. Jackson, Y. Yang, L. Hu and Y. Cui, *Nat. nanotechnology*, 2012, 7, 310-315.
58. Y. Sun, X. Hu, W. Luo, F. Xia and Y. Huang, *Adv. Funct. Mater.*, 2013, 23, 2436-2444.
59. C. Peng, B. Chen, Y. Qin, S. Yang, C. Li, Y. Zuo, S. Liu and J. Yang, *ACS nano*, 2012, 6, 1074-1081.
60. L. Zhang, H. B. Wu, S. Madhavi, H. H. Hng and X. W. Lou, *J. Am. Chem. Soc.*, 2012, 134, 17388-17391.
61. J. Zhao, F. Wang, P. Su, M. Li, J. Chen, Q. Yang and C. Li, *J. Mater. Chem.*, 2012, 22, 13328-13333.

Supporting Information

MOF-directed templating synthesis of porous multicomponent dodecahedron with hollow interiors for enhanced lithium-ion battery anodes

Chencheng Sun,[a] Jun Yang,[a] Xianhong Rui,[b] Weina Zhang,[b] Qingyu Yan,[b] Peng Chen,[c] Fengwei Huo,[a] Wei Huang,*[a] and Xiaochen Dong*[a]*

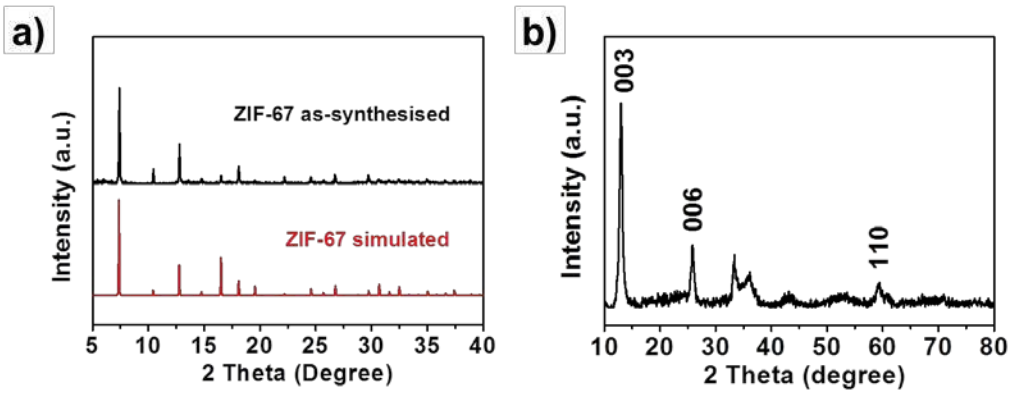

Figure S1. XRD patterns of the ZIF-67 powder (a) before and (b) after sovelenthermal treatment with 150 mg $Ni(NO_3)_2$.

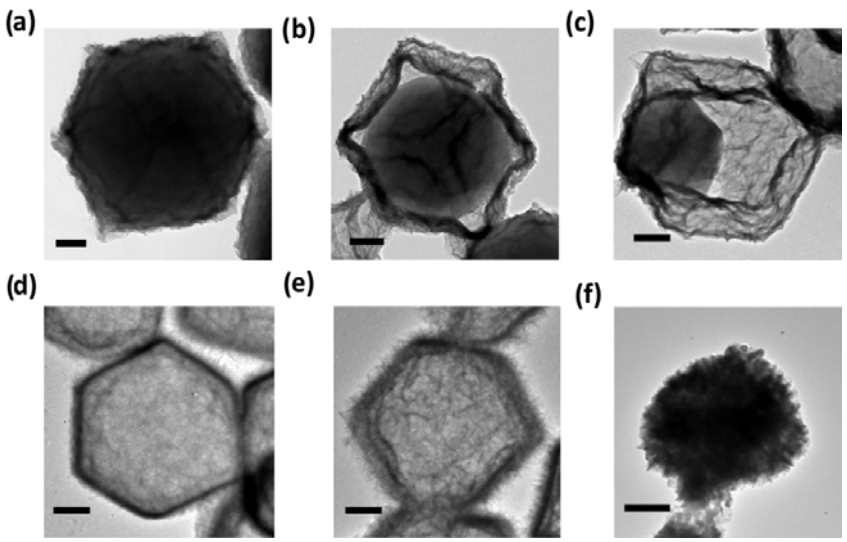

Figure S2. TEM iamges of the products obtained with different amount of $Ni(NO_3)_2$ at absolute ethanol for 1 h (a) 25 mg, (b) 50 mg, (c) 75 mg, (d) 100 mg, (e) 150 mg, (f) 500 mg, respectively. (all of the scale bars are 200 nm).

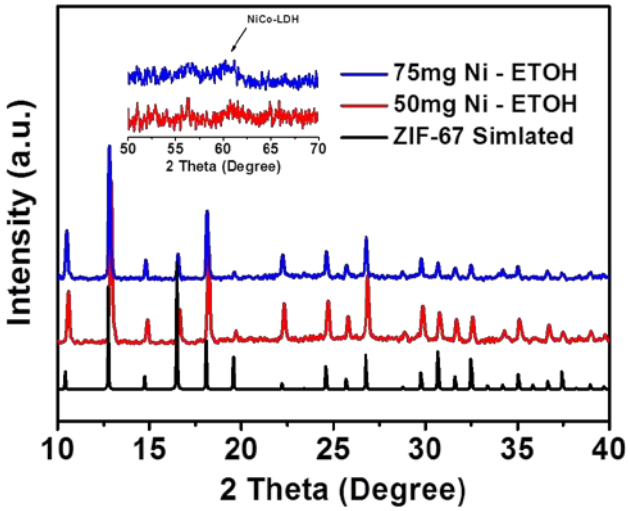

Figure S3. XRD patterns of the products obtained with 50 mg and 75 mg $Ni(NO_3)_2$ at absolute ethanol for 1 h.

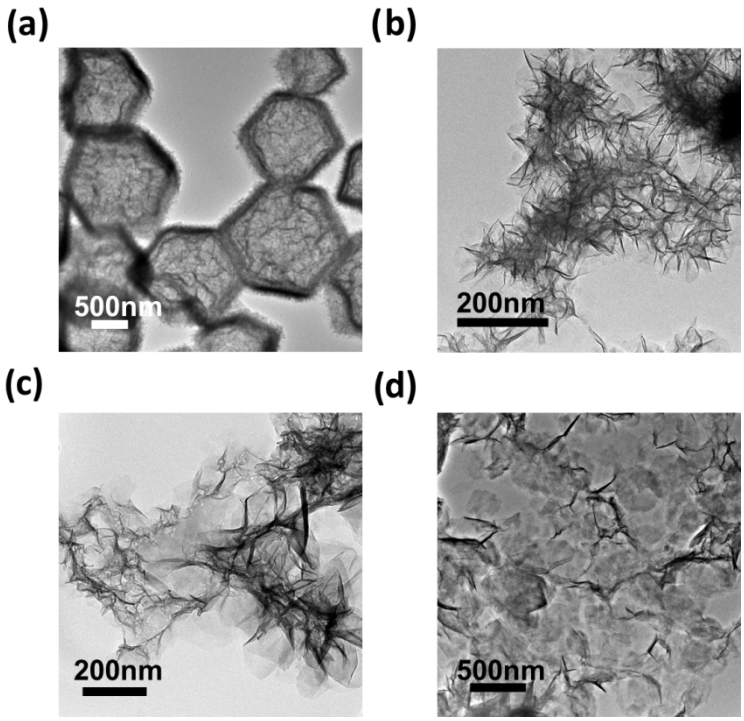

Figure S4. TEM iamges of the products obtained with different content of DI water in solvent at 90℃ for 1 h (a) 0, (b) 25%, (c) 50%, (d) 100%.

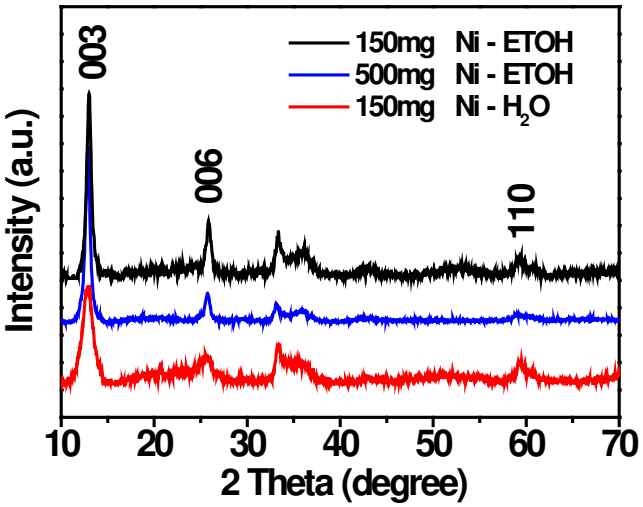

Figure S5. XRD patterns of the products obtained with various conditions. 150 mg $Ni(NO_3)_2$ at absolute ethanol (Black). 500 mg $Ni(NO_3)_2$ at absolute ethanol (Bule). 150 mg $Ni(NO_3)_2$ at DI water (Red).

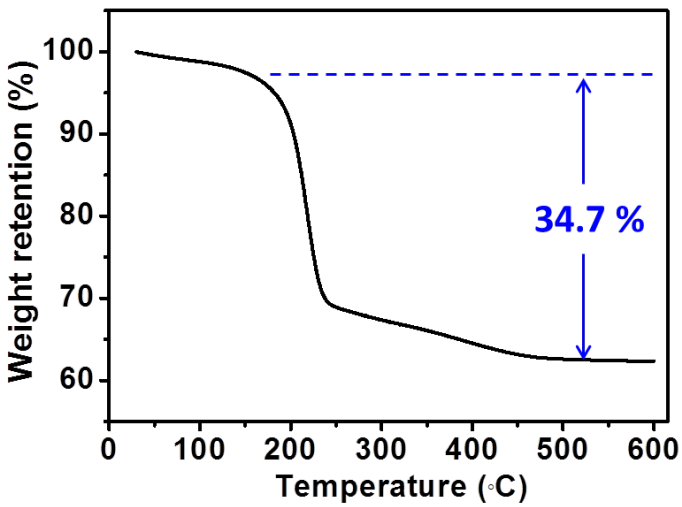

Figure S6. TGA curve of NiCo-LDH-HD obtained in the air flow at a heating rate of 2 °C min^{-1}.

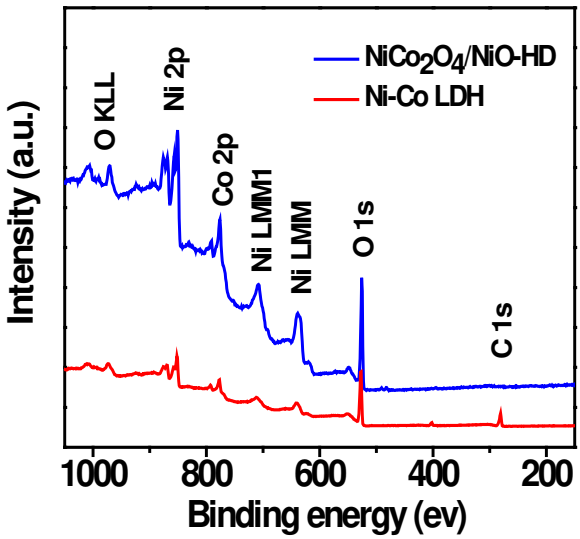

Figure S7. Survey XPS Spectrums of NiCo-LDH-HD before and after calcination in air for 1h.

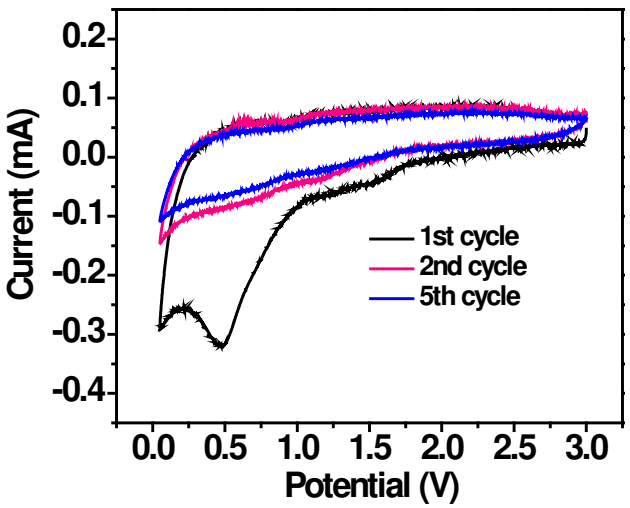

Figure S8. Representative cyclic voltammograms of ZIF-67 derived Co_3O_4 at a scan rate of 0.1 mV s^{-1} between 0.01 and 3 V *vs.* Li/Li^+.

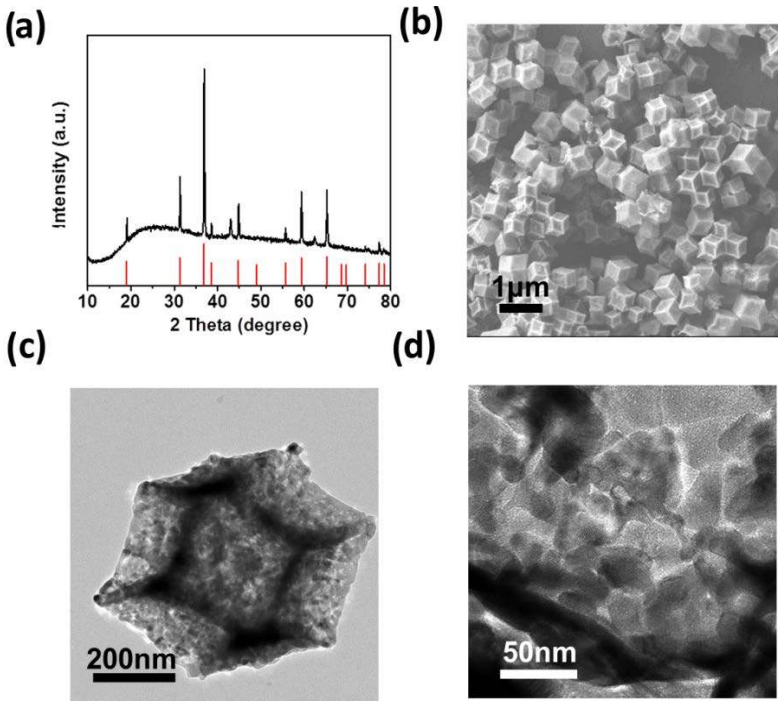

Figure S9. Characterization of CO_3O_4-HD obtained by directly calcinated ZIF-67 at air for 1h. (a) XRD pattern. (b) SEM image. (c,d) Low- and high-magnification TEM images.

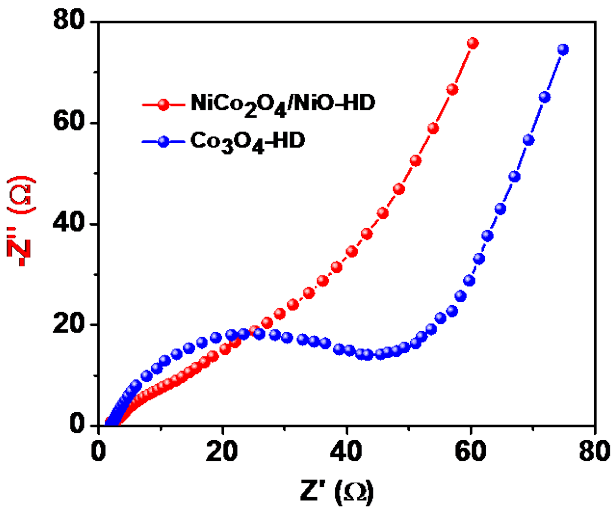

Figure S10. Electrochemical impedance spectroscopy (EIS) of $NiCo_2O_4$/NiO-HD and Co_3O_4-HD electrodes.

Table S1. Comparison of electrochemical properties as the anode materials for LIBs between various cobalt-based materials and the as-synthesized porous $NiCo_2O_4$/NiO-HD in this work.

Transition metal oxide	Specific capacity ($mAh\ g^{-1}$)	Current density ($mA\ g^{-1}$)	Cycle stability	Reference
Co_3O_4 hollow polyhedron	~1050	100	78% (100 cycles)	1
$ZnCo_2O_4$ microsphere	975	60	98% (60 cycles)	2
$MnCo_2O_4$ microbox	827	200	75.5% (50 cycles)	3
$NiCo_2O_4$ nanosheet/rGO	1034	200	87.1% (50 cycles)	4
$CuCo_2O_4$ nanoparticle	740	60	93.4% (50 cycles)	5
$CoMoO_4$ nanoflower	1021	300	87.6% (100 cycles)	6
$Co_3O_4/CoFe_2O_4$	1354	65	~90% (60 cycles)	7
Co_3O_4/Fe_2O_3 nanowires	1200	100	82% (60 cycles)	8
$ZnO/ZnCo_2O_4$ rod arrays	978	45	92% (30 cycles)	9
$NiCo_2O_4$/NiO hollow dedocahedron	1535	200	97.3% (100 cycles)	Present work

References

1 R. Wu, X. Qian, X. Rui, H. Liu, B. Yadian, K. Zhou, J. Wei, Q. Yan, X. Q. Feng and Y. Long, Small, 2014, 10, 1932-1938.

2 Y. Sharma, N. Sharma, G. Subba Rao and B. Chowdari, Adv. Funct. Mater., 2007, 17, 2855-2861.

3 L. Zhou, D. Zhao and X. W. Lou, Adv. Mater., 2012, 24, 745-748.

4 G. Gao, H. B. Wu and X. W. D. Lou, Advanced Energy Materials, 2014.

5 Y. Sharma, N. Sharma, G. V. S. Rao and B. V. R. Chowdari, J. Power Sources, 2007, 173, 495-501.

6 H. Yu, C. Guan, X. Rui, B. Ouyang, B. Yadian, Y. Huang, H. Zhang, H. E. Hoster, H. J. Fan and Q. Yan, Nanoscale, 2014, 6, 10556-10561.

7 A. K. Rai, J. Gim, T. V. Thi, D. Ahn, S. J. Cho and J. Kim, The Journal of Physical Chemistry C, 2014, 118, 11234-11243.

8 H. Wu, M. Xu, Y. Wang and G. Zheng, Nano Research, 2013, 6, 167-173.

9 C. W. Lee, S.-D. Seo, D. W. Kim, S. Park, K. Jin, D.-W. Kim and K. S. Hong, Nano Research, 2013, 6, 348-355.